British Journal of Mathematics & Computer Science
9(3): 246-260, 2015, Article no.BJMCS.2015.200
ISSN: 2231-0851

SCIENCEDOMAIN *international*
www.sciencedomain.org

Fluid Dynamics of Flow Driven by Nodal Cilia Precessing Non-circular Cones

Longhua Zhao[1*]

[1] *Department of Mathematics, Applied Mathematics and Statistics, Case Western Reserve University, Cleveland, Ohio, 44106 USA.*

Article Information

DOI: 10.9734/BJMCS/2015/17290
Editor(s):
(1) Kai-Long Hsiao, Taiwan Shoufu University, Taiwan.
(2)Mohd Zuki Salleh, Universiti Malaysia Pahang, Malaysia.
Reviewers:
(1) Anonymous, Botswana.
(2)Anonymous, Morocco.
(3)Anonymous, Malaysia.
(4)Anonymous, USA.
Complete Peer review History:
http://www.sciencedomain.org/review-history.php?iid=1144&id=6&aid=9429

Original Research Article

Received: 06 March 2015
Accepted: 14 April 2015
Published: 26 May 2015

Abstract

Nodal cilia play an important role in the left-right symmetry breaking at the early stage of the mammal embryos and show an apparent rotational motion. This study is about the flow induced by cilia sweeping out circular/elliptical cones above a no-slip plane in the low Reynolds number regime. Using the regularized Stokeslet method, we examine the properties of flows generated by a single cilium and multiple cilia, especially two cilia, which are assumed to be anchored to the embryonic heart wall. For a short-term Lagrangian fluid tracer trajectory, epicycles are presented as a nodal cilium precesses in either a circular cone or a non-circular cone shape. For the long-term behavior, the trajectory is periodic around both the circular and elliptical cones. Compared to the circular cone cases, the vertical variances are enhanced in elliptical cone cases. Besides tracer trajectories, fluid velocity fields are presented to demonstrate the flow structure. When two cilia are considered in the system, the flow structure is analyzed for the different phase angles and relative orientation of the elliptical cones.

Keywords: Stokes flow; Regularized Stokeslet Method; Nodal cilia; Lagrangian trajectory.
2010 Mathematics Subject Classification: 76A02; 74F10; 92C35

**Corresponding author: E-mail: longhua.zhao@case.edu*

1 Introduction

A cilium is a slender protuberance projecting from many cells [1, 2]. It plays a critical role in cellular motility, fluid transport and a variety of signal transduction pathways. For example, beating nodal cilia drive the directed fluid flow in the vertebrate embryos. A number of studies have been reported on this problem. The readers are referred to a review by Hamada (2008) [3] about the study of left-right asymmetry. However, it is still not fully understood how the rotating cilia drive unidirectional fluid flow in the node. Quantifying the flow generated by the nodal cilia is beneficial to understand their biomechanical properties of the biological system and especially the left-right symmetry breaking in the early development of mammals [1]. A few studies have been reported from the fluid mechanics view [4, 5, 6]. In this paper, we examine the flows induced by rotatory nodal cilia in the viscous dominated flow, i.e., in the Stokes regime.

In the Stokes regime, the singularity method seen in [7], [8], [9], and [10] has been used widely in research and is especially suitable for Stokes' problems with regular boundary geometries. The vital components for this method are to identify the type of singularities, determine the distribution and strength of the singularities, and eventually construct the velocity. Following the derivation of the fundamental singularity solution of the Stokes equations, but replacing the delta function with a smooth approximation, the method of regularized Stokeslet has been developed by Cortez [11]. The method has been very useful in many applications in areas of biological fluid flows [12]. To model fluid in the vicinity of a stationary plane boundary, Blake [13] derived the Stokeslet image system satisfying the no-slip, no-penetration condition on a flat plane. As cilia are anchored to the embryonic heart wall, we use the image system for regularized Stokeslet [14, 4] to acquire the no-slip condition for our fluid analysis.

In order to understand the microfluidic environment in embryos, an understanding of the fluid flow generated by precessing cilia is essential. Here we present a mathematical model and numerical method that solves the Stokes equations of zero Reynolds number flow with the precession of cilia emanating from a planar wall in 3D. Three different shapes of the cone are considered and compared. After computing the velocity field due to a collection of forces applied over the cilia, we explore the fluid tracer trajectory.

2 Model of Nodal Cilia Sweeping Cones

In this study, we explore the fluid flow induced by nodal cilia attached to a flat plane wall and precessing cones in a viscous dominated fluid. We utilize the method of regularized Stokeslet and the image system previously derived for the method of regularized Stokeslet to account for the presence of a plane wall [11, 15, 14]. Below we briefly discuss the equations of motion in this viscous regime, the method of regularized Stokeslet and its image system, and the prescribed position and motion of the cilium.

The governing equations are the incompressible Stokes equations [9, 16, 17],

$$\begin{aligned} \mu\nabla^2\mathbf{u} - \nabla p + \mathbf{f} &= 0, \\ \nabla\cdot\mathbf{u} &= 0, \end{aligned} \tag{2.1}$$

where $\mathbf{u}$ is the velocity of the fluid, ∇p the gradient of the pressure, μ is the dynamic viscosity, and $\mathbf{f}$ is the extern force due to the cilium.

2.1 Stokeslet

One analytical tool for obtaining solutions to Stokes equations is singularity theory [18, 19, 7, 9]. The basis is to construct solutions to particular boundary value problems through the superposition of

fundamental solutions. Fundamental solutions are found by solving Stokes equations with singular force in an unbounded domain. The primary fundamental solution, called the Stokeslet [7], is constructed by applying a point force, represented by the three-dimensional Dirac delta function $\delta(\mathbf{x})$, to the Stokes flow field. The Stokeslet velocity field

$$\mathbf{u}(\mathbf{x}-\mathbf{s};\boldsymbol{\alpha}) = \frac{\boldsymbol{\alpha}}{|\mathbf{x}-\mathbf{s}|} + \frac{[\,\boldsymbol{\alpha}\cdot(\mathbf{x}-\mathbf{s})\,]\,(\mathbf{x}-\mathbf{s})}{|\mathbf{x}-\mathbf{s}|^3} \tag{2.2}$$

satisfies the steady, free space, singularly-forced Stokes equations

$$\begin{aligned} \mu\nabla^2\mathbf{u} + 8\pi\,\mu\,\boldsymbol{\alpha}\,\delta(\mathbf{x}-\mathbf{s}) &= \nabla p, \\ \nabla\cdot\mathbf{u} &= 0. \end{aligned} \tag{2.3}$$

The vectors $\boldsymbol{\alpha}$ and $\mathbf{s}$ characterize the Stokeslet's strength and location, respectively. Fundamental solutions are also called singularity solutions. Since the Stokes equations are linear, higher order singularities can be constructed through derivatives of the Stokeslet solution with the corresponding singular, external, applied force being the equivalent derivative of the point force $8\pi\,\mu\,\boldsymbol{\alpha}\,\delta(\mathbf{x}-\mathbf{s})$. Thus, higher order singularities, such as Stokes doublets and point-force dipoles, become available to singularity theory for building solutions to Stokes flow boundary value problems [7].

2.2 Regularized Stokeslet Method

The regularized Stokeslet method [11] is based on the smoothing of the forces and itself has a wide applicability. The resulting expressions provide the pressure and velocity field as functions of the forcing. The relation between the velocity and force is inverted to find the forces that impose a given velocity boundary condition or to compute the velocity with the given forces directly. Numerically, this forms the relation in an explicit linear system.

The approach is to consider the forces to be applied over a small ball, where they vary smoothly from a maximum value at the center to zero on its surface, rather than being concentrated at points (as Dirac measures for the Stokeslet). The radius of the support of the forces is a parameter that can be controlled independently with given boundary discretization. Similar to Stokeslet, the regularized Stokeslet is a fundamental solution to

$$\begin{aligned} \mu\nabla^2\mathbf{u} + \boldsymbol{f}_0\,\phi_\varepsilon(\mathbf{x}-\mathbf{s}) &= \nabla p, \\ \nabla\cdot\mathbf{u} &= 0. \end{aligned} \tag{2.4}$$

where $\phi_\varepsilon(\mathbf{x}-\mathbf{s})$ is a radially symmetric smooth function with the property that $\int \phi_\varepsilon(\mathbf{x})d\mathbf{x} = 1$. These functions are called *blobs* or *cutoffs*. Fig. 1 shows a typical blob with different values of ε, which control the width, or spreading. A smaller ε is, the tighter and taller the integrand $\phi_\varepsilon(\mathbf{x})$ will be. In the limit $\varepsilon \to 0$, the blob approaches a Dirac delta.

The regularized Stokeslet is the velocity field

$$\mathbf{u} = \frac{\mathbf{1}}{\mu}\left[(\mathbf{f_0}\cdot\nabla)\nabla\mathbf{B}_\varepsilon - \mathbf{f_0}\mathbf{G}_\varepsilon\right], \tag{2.5}$$

where $G_\varepsilon(\mathbf{x})$ is the solution of $\nabla^2 G_\varepsilon = \phi_\varepsilon(\mathbf{x})$ in infinite space and $B_\varepsilon(\mathbf{x})$ is the solution of $\nabla^2 B_\varepsilon = G_\varepsilon(\mathbf{x})$ in infinite space. The function $G_\varepsilon(\mathbf{x})$ is a smooth approximation of the Green's function

$$G(\mathbf{x}) = -\frac{1}{4\pi}\frac{1}{|\mathbf{x}|}, \qquad \text{in } \mathbb{R}^3, \tag{2.6}$$

for $|\mathbf{x}| > \varepsilon$. And,

$$B(\mathbf{x}) = -\frac{|\mathbf{x}|}{8\pi}, \qquad \text{in } \mathbb{R}^3, \tag{2.7}$$

is the solution of the biharmonic equation $\nabla^2 B(\mathbf{x}) = \delta(\mathbf{x})$. For our choice of the blob

$$\phi_\varepsilon(\mathbf{x}) = \frac{15\varepsilon^4}{8\pi\left(|\mathbf{x}|^2+\varepsilon^2\right)^{7/2}}, \tag{2.8}$$

the resulting velocity field is

$$\mathbf{u} = \frac{\mathbf{1}}{\mathbf{8}\pi\mu}\left[\mathbf{f_0}\frac{\mathbf{2}\varepsilon^{\mathbf{2}}+\mathbf{x^2}}{\left(|\mathbf{x}|^{\mathbf{2}}+\varepsilon^{\mathbf{2}}\right)^{\mathbf{3/2}}} - \frac{(\mathbf{f_0}\cdot\mathbf{x})\mathbf{x}}{\left(|\mathbf{x}|^{\mathbf{2}}+\varepsilon^{\mathbf{2}}\right)^{\mathbf{3/2}}}\right]. \tag{2.9}$$

In particular to the numerical simulation in this paper, the system is based on totally N point forces distributed along the centerline of the nodal cilium. In the governing equations (2.1), the extern force $\mathbf{f} = \sum_{k=1}^{N} \mathbf{f}_k \phi_\varepsilon$ due to the cilium. With N point forces, f_k centered at $\mathbf{x}_k$ $(k = 1, \cdots, N)$, the pressure and velocity can be directly computed by as a linear combination of those point forces

$$\mathbf{u}(\mathbf{x}) = \frac{1}{\mu}\sum_{k=1}^{N}\left[(\mathbf{f}_k\cdot\nabla)\nabla B_\varepsilon(\mathbf{x}-\mathbf{x}_k) - \mathbf{f}_k G_\varepsilon(\mathbf{x}-\mathbf{x}_k)\right], \tag{2.10}$$

$$p(\mathbf{x}) = \sum_{k=1}^{N}\mathbf{f}_k\cdot\nabla G_\varepsilon(\mathbf{x}-\mathbf{x}_k). \tag{2.11}$$

As G_ε and B_ε are given smooth functions, the obtained velocity and pressure from (2.10)-(2.11) for the flow field are explicit formulas. And, the resulted velocity field in this approach is mesh-free.

2.3 Image System for a Stokeslet

Instead of studying the system in the free space, it is important to consider the wall-effect to the fluid flow. To enforce no-slip boundary conditions on the wall, the method of images is commonly implemented to handle the no-slip plane. The image system for the singular Stokeslet near a plane wall was obtained by Blake [13]. It is a sum of singularity solutions (Stokeslet, Stokeslet doublet and Stokeslet potential dipole) evaluated at the image point. The image system of regularized Stokeslet near a plane wall was previously derived in [14]. It is the combination of the regularized Stokeslet, regularized Stokeslet doublet, regularized Stokeslet potential dipole, and, different from the singular image system, also includes the regularized Rotlet. In this study, we use the blobs and regularized singularity solutions in the forms found in [14, 20].

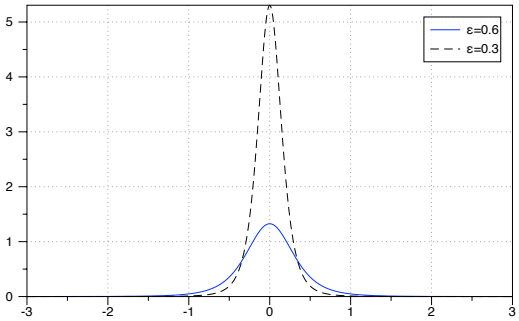

Figure 1: Typical blob for two different values of ε.

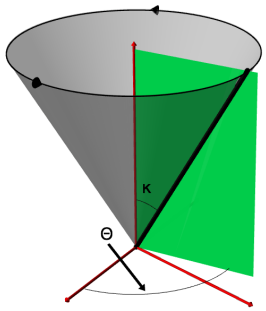

Figure 2: Circular cone

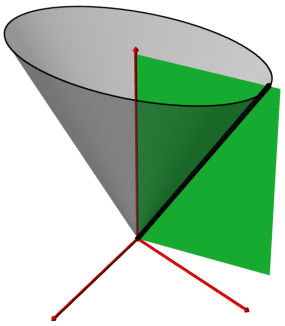

Figure 3: Elliptical cone

2.4 Prescribed Motion of Nodal Cilia

To model the flow driven by nodal cilia, we distribute singularities along the centre-line (i.e., the axis of the cilium) and prescribe the rotatory motion of the cilium. Two types of cones swept out by the nodal cilia are shown in Fig. 2 and 3. In the figures, the cilium is depicted as the black slim body along the surface of the cone. The base of the cilium is anchored at the origin of the coordinate. The horizontal axis plane is the no-slip plane in the system. At any instantaneous time, the position of the cilium is uniquely defined by cone angle κ, and azimuthal angle θ for an upright cone. The cone angle, κ, is the angle from the axis of the cone to the centerline of the cilium. In others work, it sometimes is referred as the semi-cone angle. For circular cones, cone angle κ is constant. For elliptical cones, cone angle κ varies while the cilium sweeps along the cone.

Assume the length of the cilium is ℓ. Using standard rotation matrices, the centerline of an idealized-straight nodal cilium is defined in different frames used in this paper:

- In the body frame where the cilium is along the positive x-axis: $\mathbf{x}_{sb} = (s, 0, 0)^T, \quad 0 < s < \ell$.
- In the tilted body frame where the cilium is titled with the cone angle κ in the xz-plane: $\mathbf{x}_{s0} = (s\sin\kappa, 0, s\cos\kappa)^T$, $\mathbf{x}_{s0} = R_\kappa \mathbf{x}_{sb}$. The transformation matrix R_κ is

$$R_\kappa = \begin{pmatrix} \sin\kappa & 0 & -\cos\kappa \\ 0 & 1 & 0 \\ \cos\kappa & 0 & \sin\kappa \end{pmatrix}. \tag{2.12}$$

- In the frame where the cilium is sweeping an upright cone:

$$\mathbf{x}_{st} = (s\sin\kappa\cos\Theta(t), s\sin\kappa\sin\Theta(t), s\cos\kappa)^T, \text{ or } \mathbf{x}_{st} = R_{\omega\phi}\mathbf{x}_{s0}, \tag{2.13}$$

  in which

$$R_{\omega\phi} = \begin{pmatrix} \cos\Theta(t) & \sin\Theta(t) & 0 \\ \sin\Theta(t) & \cos\Theta(t) & 0 \\ 0 & 0 & 1 \end{pmatrix}. \tag{2.14}$$

  Eqn. (2.13) describes the position of the cilium as a function of time. $\Theta(t)$ depends on the frequency of the rotation and the phase angle ϕ.

Suppose that the trace of the cilium fall on the surface of the elliptical cone

$$\frac{x^2}{a^2} + \frac{y^2}{b^2} = z^2. \tag{2.15}$$

For elliptical cones, we assume the cilium is sweeping along the surface of the elliptical cone with a constant rate in the elliptic coordinate, i.e., the polar angle is $\omega t + \phi$, where ϕ is the given phase angle from the reference position. In our simulations, the positive x-axis is used for this reference position. Then the azimuthal angle of the cilium is

$$\Theta = \arccos\left(\frac{a\cos(\omega t+\phi)}{\sqrt{a^2\cos^2(\omega t+\phi)+b^2\sin^2(\omega t+\phi)}}\right)+\pi\,\mathrm{floor}\left(\frac{\omega t+\phi}{\pi}\right). \tag{2.16}$$

Moreover, the cone angle κ satisfies

$$\tan\kappa = \sqrt{a^2\cos^2(\omega t+\phi)+b^2\sin^2(\omega t+\phi)}. \tag{2.17}$$

For a nodal cilium sweeping an elliptical above a no-slip plane, the cone angle $0 < \kappa \leq \pi/2$. Therefore,

$$\kappa = \arctan\sqrt{a^2\cos^2(\omega t+\phi)+b^2\sin^2(\omega t+\phi)}. \tag{2.18}$$

To determine the velocity field of the flow, the no-slip boundary condition for the surface of the cilium is imposed to the system. Given the position of the cilium in time, the velocity of the cilium is founded by differentiating its position with respect to t. Then,

$$\frac{d\mathbf{x}_s}{dt} = \dot{R}_{\omega\phi}R_\kappa\mathbf{x}_{sb} + R_{\omega\phi}\dot{R}_\kappa\mathbf{x}_{sb}. \tag{2.19}$$

Since R_κ and $R_{\omega\phi}$ are given in Eqn. (2.12) and (2.14), the velocity of the cilium is

$$\mathbf{u} = \frac{d\mathbf{x}_s}{dt} = \begin{pmatrix} -\sin\Theta(t) & -\cos\Theta(t) & 0 \\ \cos\Theta(t) & -\sin\Theta(t) & 0 \\ 0 & 0 & 0 \end{pmatrix} R_\kappa\mathbf{x}_{sb}\frac{d\Theta}{dt} \tag{2.20}$$

$$+R_{\omega\phi}\begin{pmatrix} \cos\kappa(t) & 0 & \sin\kappa(t) \\ 0 & 0 & 0 \\ -\sin\kappa(t) & 0 & \cos\kappa(t) \end{pmatrix}\mathbf{x}_{sb}\frac{d\kappa}{dt}, \tag{2.21}$$

where $\frac{d\kappa}{dt}$ and $\frac{d\Theta}{dt}$ are computed from Eqn. (2.18) and (2.16), respectively.

3 Results

Based on the model built in the paper, the velocity field of the flow field is expressed as a linear combination of the regularized Stokeslet and corresponding image systems. The strength of the regularized Stokeslet is determined by the boundary condition on the surface of the cilium. After the velocity field is obtained, the fluid tracer trajectory is computed as an initial value problem, numerically. First we will show the trajectory of a single fluid tracer for different cone figurations.

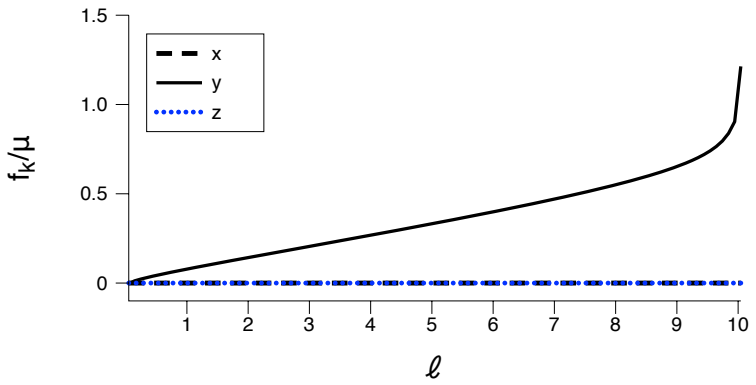

Figure 4: Force distribution on the centerline of the cilium as it sweeps along an elliptical cone ($a = b/10 = \tan(\pi/6)$).

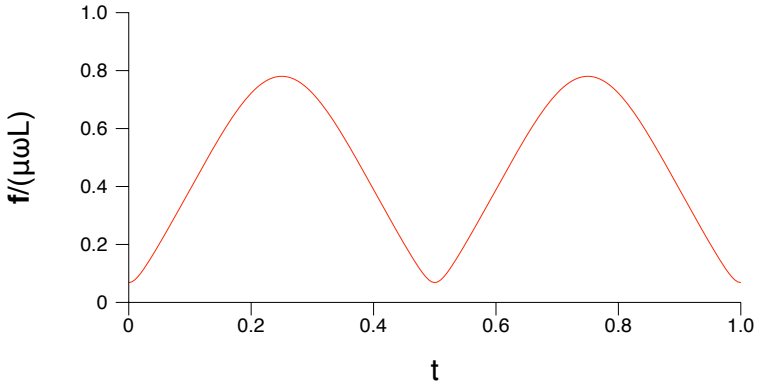

Figure 5: Normalized total force $\mathbf{f}/(\omega L)$ over one period.

Then, the system with multiple cilia, especially two cilia, will be studied to show the flow structure. To explore the flow induced by multiple cilia, we will analyze effects of phase difference and the relative orientation of elliptical cones.

In the simulations, the geometry of the cilium will be fixed. We set that the length of the cilium is $\ell = 10$ and its cross-section radius is 0.05, which is also the value of the regularization parameter ϵ used in Eqn. (2.9). The shape of the cone is controlled by parameters a and b in Eqn. (2.15).

As the strength is important information about the drag force the cilium experiences, we present the force distribution in Fig. 4 and 5. The force varies its direction and magnitude over time, however the properties are similar. Fig. 4 shows the force distribution $\mathbf{f}_k$ on the cilium at the position $t = 0$, when the cilium is sweeping out an elliptical cone. At this position, the force strength components in the x and z direction are almost negligible, compared to the y component. Fig. 5 shows the total force $\mathbf{f}$, which is found by integrating the force acting on each point on the cilium, during one period of the motion. The total force is normalized by the length of the cilium ℓ and the rotation ration parameter ω.

3.1 Lagrangian Fluid Tracer Trajectory with One Cilium

To qualitatively study flow properties, the Lagrangian fluid tracer trajectories are explored. Fig. 6-10 show the trajectory of a fluid tracer when a single cilium rotates above a no-slip plane. The initial positions of the fluid tracer are set the same for all three different cones. For the circular cone, $a = b = \tan(\pi/6)$, which sets cone angle $\kappa = \pi/6$. The initial position of the trace is $(x, y, z) = (0, 3, 8)$ and marked as a green dot on the trajectory. The end point of the trajectory is marked as a red dot. The values for other parameters are frequency $\omega = 2\pi$ and phase angle $\phi = 0$. Fig. 6 and 7 show two views of a trajectory when the cilium sweeps on an upright circular cone. While the cilium rotates, the fluid tracer moves along a slow, large, periodic orbit surrounding the cone. The epicycles on the trajectory are with a time scale proportional to one revolution of the cilium [21, 5]. Except for the fluctuation during each epicycle, the fluid tracer stays at a fixed z-level. This property is illustrated clearly from the side view of the trajectory in Fig. 7 and the plot of z component of this trajectory in Fig. 12. This can be confirmed by the Poincare map [6]. The Poincare map is a plot of the trajectory through a vertical plane in the body frame, where the cilium is fixed and the background flow is purely rotating flow. The Poincare map of this trajectory is a dot.

Figs. 8-9 and 10-11 show trajectories when the cilium sweeps on upright elliptical cones $a = 2b = \tan(\pi/6)$ and $a = 10b = \tan(\pi/6)$, respectively. For elliptical cone $a = 2b = \tan(\pi/6)$, the maximum cone angle is $\kappa = \frac{\pi}{6}$ and the minimum cone angle is $\kappa = \frac{\pi}{12}$. From these trajectories, the epicycle and periodicity of the trajectories around the cone also clearly show up. Similarly, each epicycle is roughly corresponding to one rotation of the cilium and the orbit is surrounding the elliptical cone. From the top views, the trajectories of the fluid tracer are deformed consistently as shapes of the cone. When the cone is circular, the trajectory is circular in a long period of time. For elliptical cones, the trajectory is elliptical in the long term.

Besides the deformation shown in the top view, we see the tracer behaves differently in the vertical direction from the side view. Fig. 12 and 13 show vertical components of three trace trajectories in Figs. 8-11. In Fig. 12, the red dotted curve is for the z component the trajectory with the circular cone shown in Fig. 6-7, and the black curve is for the z component of the trajectory with elliptical cone $a = 2b = 1$ shown in Fig. 8-9. The horizontal axis T is referred to the number of rotations of the cilium. The vertical variance of the trajectory when a cilium sweeps on the elliptical cones is enhanced compared to the circular cone. There are two periodicities of the vertical components for elliptical cones situations. The first one is due to the periodicity of rotation of the cilium and the second is due to the time variance of the cone angle κ for elliptical cones.

3.2 Velocity Field

On the surface of the ciliated ventral node of the developing embryo, the interaction of the cilia are extremely important to the proper direction of fluid. We check the velocity field for different alignments of the cilia in the flow. For multiple cilia presenting in the system, the symmetry property of the cone is broken. We focus on analyzing the phase difference for multiple cilia sweeping cones.

Figs. 14-16 show the instantaneous velocity field computed on a horizontal surface with a single cilium or two cilia sweeping. The horizontal surface is at $z = 10$ for these figures. The cone angle is $\kappa = \pi/6$ and the geometry of the cilium is the same as in the previous subsection. For two-cilium cases, phase angles for cilia are randomly chosen for each scenario.

Fig. 14 shows the velocity field for flow induced by a single cilium.

Figs. 15 and 16 show velocity fields with two cilia precessing. These two cilia are anchored at (-5,0) and (5,0) on the no-slip plane (the z-plane). Since phase angles are randomly chosen, these are only two scenarios.

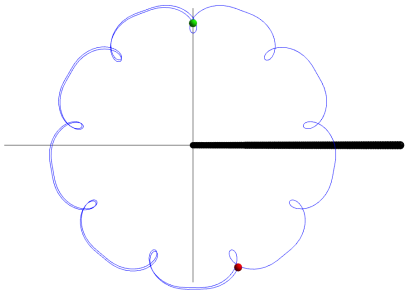

Figure 6: Circular ($a = b$): top view

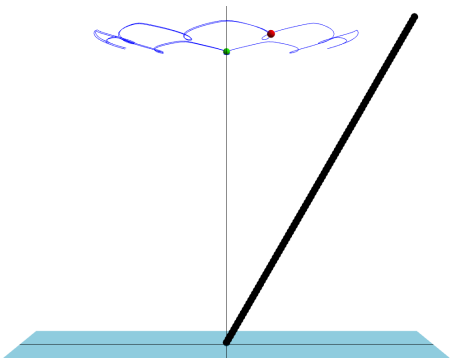

Figure 7: Circular ($a = b$): side view

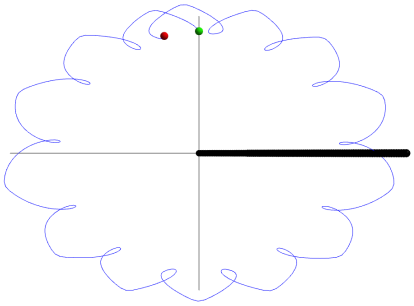

Figure 8: Elliptic ($a = 2b$): top view

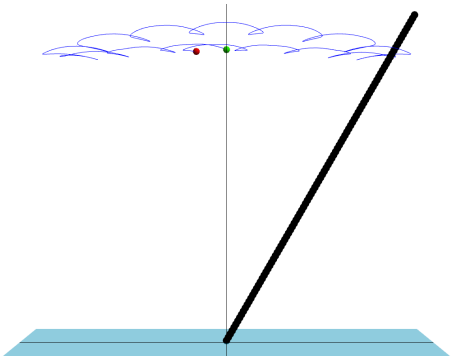

Figure 9: Elliptic ($a = 2b$): side view

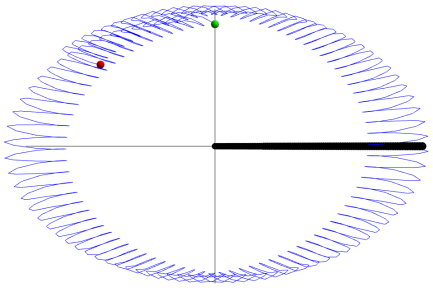

Figure 10: Elliptic ($\frac{a}{b} = 10$): top view

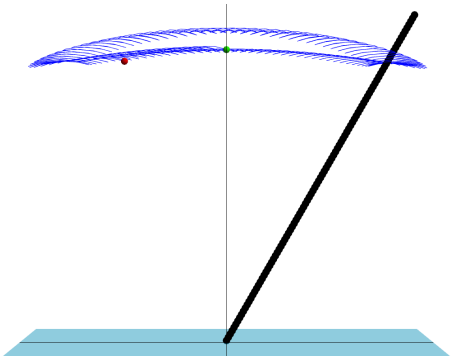

Figure 11: Elliptic ($\frac{a}{b} = 10$): side view

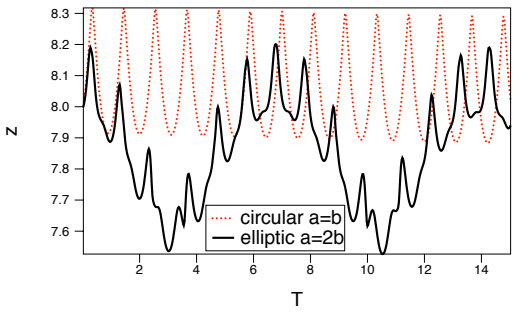

Figure 12: Vertical variance

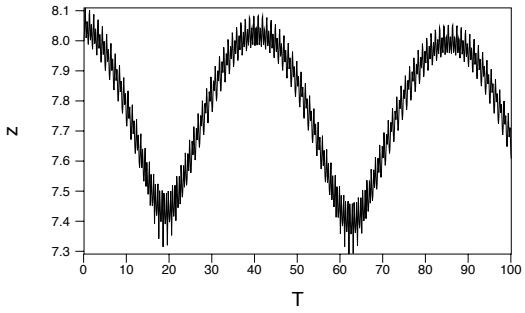

Figure 13: Vertical variance for $\frac{a}{b} = 10$.

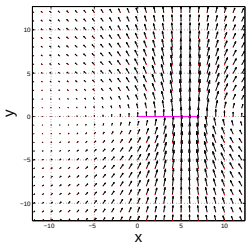

Figure 14: Single cilium.

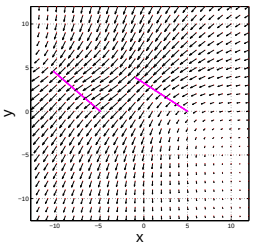

Figure 15: Two cilia.

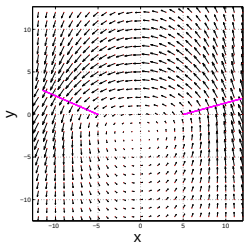

Figure 16: Two cilia

With these two samples, the velocity field shows that there are directional flows as Fig. 15 and also circulation as Fig. 16 in the near field.

Fig. 17 shows velocity fields of flow driven by with 2×2 cilia. For all three scenarios, cilia are anchored at (-5, -5), (-5,5), (5,-5) and (5,5) on the no-slip plane. Phase angles for four cilia are also randomly values. Rivers and whirlpools appear in the flow fields.

3.3 Properties of Fluid Tracer Trajectories with Multiple Cilia

To explore the tracer trajectory with multiple cilia, we consider two cilia in the system. In many biology systems, cilia move in a coordinated fashion in either complete synchrony or by maintaining a constant phase difference [1]. The frequency of sweeping is set the same for all cilia.

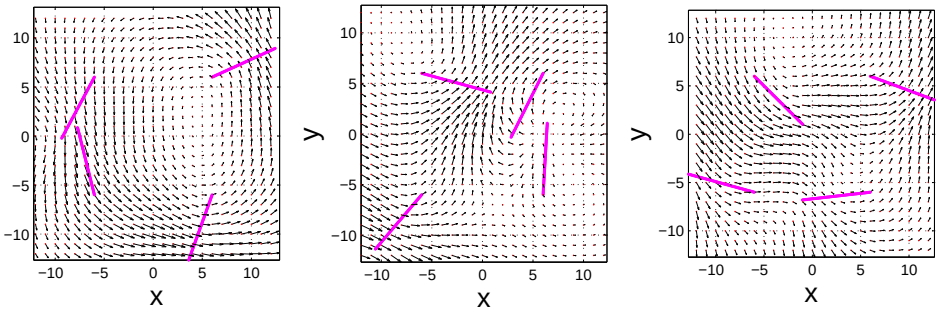

Figure 17: Velocity field for 2×2 cilia.

Figs. 18 and 19 are the top view and the side view of a tracer trajectory in the flow generated by two cilia precessing circular cones. The frequencies of the rotation for these two cilia are same. The phase difference between two cilia is zero, which means the cilia start at the same relative location on the cones. For this trajectory, both cilia are initialized in the x-z plane as shown in the figures.

Figs. 20-21 show tracer trajectories when two cilia sweep out circular cones but with the phase difference $\phi = \pi/2$, and π, respectively. Since the trajectory is almost planar as Figs. 18-19, only top views are presented for these cases.

Figs. 22 and 23 are views of a tracer trajectory when two cilia sweep out elliptical cones. For both elliptical cones, $a = 2b = 1$ and the phase difference is zero.

These plots demonstrate the importance of phase difference for flows. It is interesting to see that the periodic tracer trajectory is deformed more when changing the phase angle than changing the shape of the cone.

As the elliptical cone has its orientation based on the major axis and minor axis, we check the trajectory for a fluid trace with different orientations of the elliptical cones. Figs. 24-29 show fluid tracer trajectories when two cilia sweep elliptical cones, whose major axises are perpendicular to each other. For the green cilium (on the left), $a = 2b = 1$. For the black cilium (on the right), $2a = b = 1$. For these three pairs of views (3D and top) in Figs. 24-29, the phase differences are 0, $\pi/2$ and π, respectively. These phase differences can be checked from two views of the cilia. These figures illustrate that, given the configuration of the cones, the phase difference affects the shape of the epicycles rather than the long-term orbits.

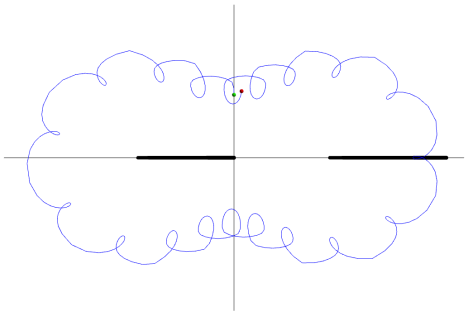

Figure 18: Circular cone $a = b$

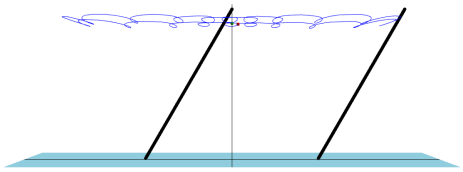

Figure 19: Side view of Fig. 18

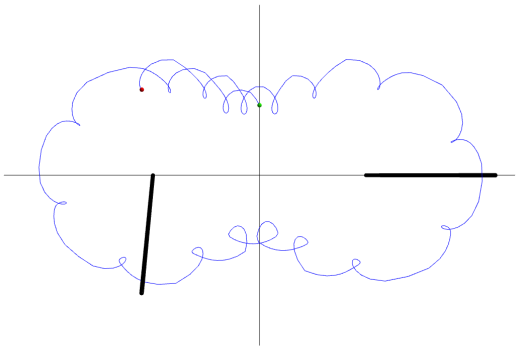

Figure 20: Circular cone $\phi = \pi/2$

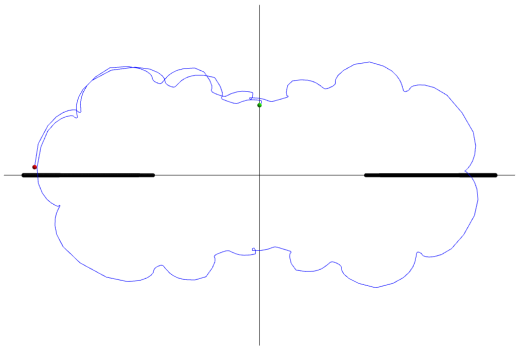

Figure 21: Circular cone $\phi = \pi$

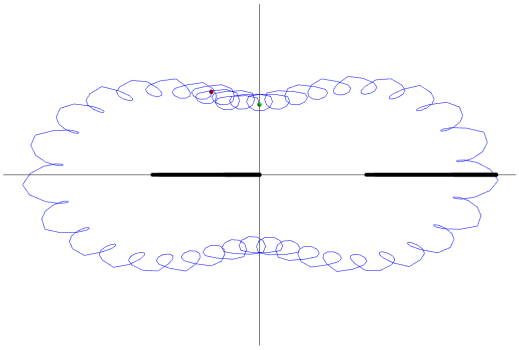

Figure 22: Elliptic cones $a = 2b$

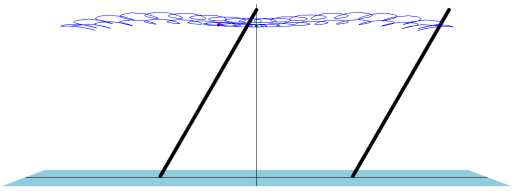

Figure 23: Side view of Fig. 22

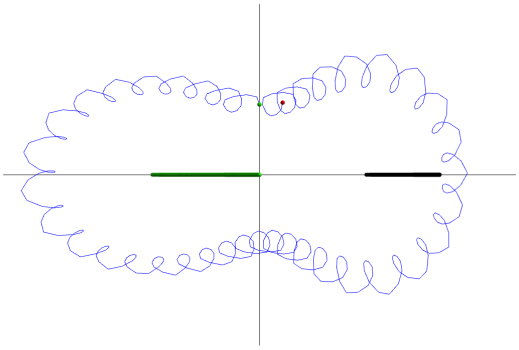

Figure 24: Black cilium: $a = 2b = 1$, green cilium: $2a = b = 1$, zero phase difference

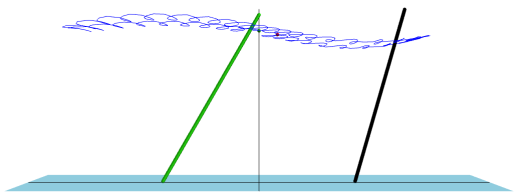

Figure 25: Side view of Fig. 24

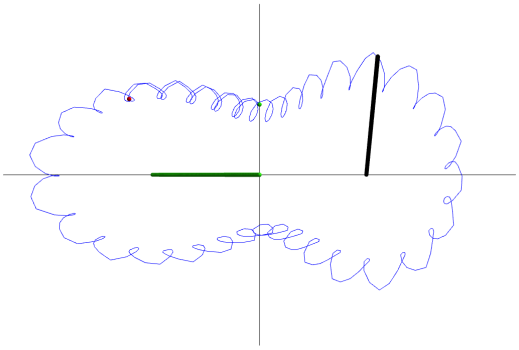

Figure 26: Black cilium: $a = 2b = 1$, green cilium: $2a = b = 1$, phase difference $\frac{\pi}{2}$

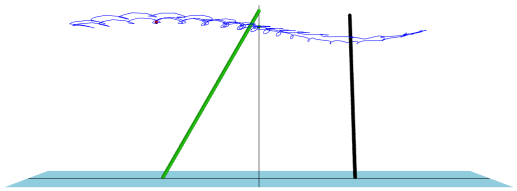

Figure 27: Side view of Fig. 26

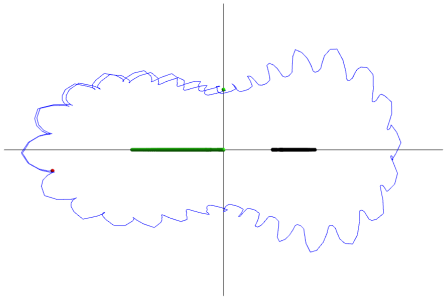

Figure 28: Black cilium: $a = 2b = 1$, green cilium: $2a = b = 1$, phase difference π

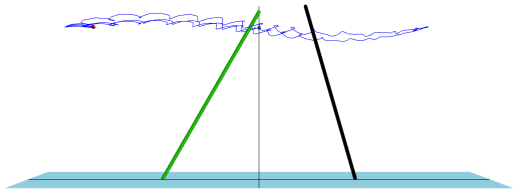

Figure 29: Side view of Fig. 28

Conclusions

In this study, we have considered the flow driven by nodal cilia with prescribed motions. This study can be used to gain insight into the left-right symmetry breaking during embryo development. We have formulated a model describing the motion of a fluid tracer in the flow. Using the method of regularized Stokeslet and its image system to our model, the velocity field in a viscous fluid flow due to non-circular rotatory cilia precessing above a no-slip flat wall has been computed. The motion of the tracer in the fluid is then attained with the forward Euler method. The numerical results show that the model successfully captures epicycles and large periodic orbits surround the cones from the tracer trajectory. These epicycles and large orbits had been observed in the flow experiments [6]. We have found that when cilia sweep elliptical cones, the vertical variance of tracer trajectories is enhanced. Additionally, we have demonstrated the fluid velocity field and properties of trajectories with multiple cilia precessing.

A natural extension of this study is the generalization to a periodic lattice of cilia attached to a surface. More thorough study about the variance of the rotation frequency and the phase difference would also be interesting. Moreover, the results reported in this paper are for cilia sweeping upright cones. When the cone is tilted, the symmetry between the cone and the no-slip plane is broken. The tilted rotation and directional flow are close related. Efforts have been made to investigate new phenomena introduced by the tilt. Such results will be reported in the future work. Furthermore, motions of the cilia are prescribed in this paper. A future study of the cilia motion based its microstructure coupled with the fluid mechanics would be useful. Ultimately we would like to model unidirectional fluid transport driven by cilia movement.

Competing Interests

The author declares that no competing interests exist.

References

[1] Nonaka S, Yoshiba S, Watanabe D, Ikeuchi S, Goto T, Marshall WF, Hamada H. De novo formation of leftright asymmetry by posterior tilt of nodal cilia. PLoS Biol. 2005;3(8):e268.

[2] Babu D, Roy S. Left-right asymmetry: Cilia stir up new surprises in the node. Open Biology. 2013;3(5).

[3] Hamada H. Breakthroughs and future challenges in left-right patterning. Develop. Growth Differ. 2008;50:S71-S78.

[4] Smith DJ. A boundary element regularized Stokeslet method applied to cilia- and flagella-driven flow.Proceedings of the Royal Society of London A: Mathematical, Physical and Engineering Sciences. 2009;465(2112):3605-3626.

[5] Smith DJ, Blake JR, Gaffney EA. Fluid mechanics of nodal flow due to embryonic primary cilia. Journal of The Royal Society Interface. 2008;5:567-573.

[6] Zhao L. Fluid-structure interaction in viscous dominated flows. PhD thesis, the University of North Carolina at Chapel Hill, July; 2010.

[7] Chwang AT, Wu TY. Hydromechanics of low-Reynolds-number flow. Part 2. Singularity Method for Stokes Flows. J. Fluid Mech. 1975;67:787-815.

[8] Kim S, Karrila SJ. Microhydrodynamics: Principles and selected applications. Dover Publications; 2005.

[9] Pozrikidis C. Introduction to theoretical and computational fluid dynamics. New York: Oxford University Press; 1997.

[10] Leal LG. Particle motions in a viscous fluid. Ann. Rev. Fluid Mech. 1980;12:435-476.

[11] Cortez R. The method of regularized stokeslets. SIAM J. Sci. Comput. 2001;23:1204.

[12] Buchmann A, Fauci L, Leiderman K, Strawbridge E, Zhao L. Flow induced by bacterial carpets and transport of microscale loads. Applications of Dynamical Systems in Biology and Medicine, The IMA Volumes in Mathematics and its Applications; 2014.

[13] Blake JR. A note on the image system for a Stokelet in a no-slip boundary. Proceedings of the cambridge philosophical society. 1971;70:303-310.

[14] Ainley J, Durkin S, Embid R, Boindala P, Cortez R. The method of images for regularized stokeslets. Journal of Computational Physics. 2008;227:4600-4616.

[15] Cortez R, Fauci L, Medovikov A. The method of regularized Stokeslets in three dimensions: Analysis, validation, and application to helical swimming. Phys. Fluids. 2005;17:031504.

[16] Batchelor GK. An Introduction to fluid dynamics. Cambridge University Press; 2000.

[17] Leal LG. Advanced transport phenomena: Fluid mechanics and convective transport processes. Cambridge University Press; 2007.

[18] Burgers JM. On the motion of small particles of elongated form, suspended in a viscous fluids. Nordemann Publishing, New York; 1938.

[19] Batchelor GK. Slender-body theory for particles of arbitrary cross-section in stokes flow. J. Fluid Mech. 1970;44:419-440.

[20] Cortez R, Varela D. A general system of images for regularized Stokeslets and other elements near a plane wall. Journal of Computational Physics. 2015;285(0):41-54.

[21] Bouzarth EL, Brooks A, Camassa R, Jing H, Leiterman TJ,. Mclaughlin RM, Superfine R, Toledo J, Vicci L. Epicyclic orbits in a viscous fluid about a precessing rod: Theory and experiments at the micro- and macro-scales. Physical Review E. 2007;76(1).

Peer-review history:
The peer review history for this paper can be accessed here (Please copy paste the total link in your browser address bar)
www.sciencedomain.org/review-history.php?iid=1144&id=6&aid=9429